Journal of Directed Energy, **4**, Fall 2010, 98–109

Characterization of a Multikilowatt, Yb:YAG, Ceramic Thin-Disk Laser

Ahmed Lobad[1] and Don Stalnaker

Boeing LTS Inc., P.O. Box 5670, MC RN-M1, Kirtland AFB, New Mexico 87185

and

L.A. (Vern) Schlie

Integral Laser Solutions, Albuquerque, New Mexico 87114

and

T. Sean Ross and William P. Latham*

AFRL/RD, Directed Energy Directorate, 3550 Aberdeen Blvd. SE, Kirtland AFB, New Mexico 87117

The operation of a 1030-nm, single thin-disk laser, which produced 6.5 kW of laser output power with 57% slope efficiency is reported. The Yb:YAG ceramic gain element is 200 μm thick, and bonded to a 1-mm thick, undoped ceramic YAG cap. The gain element is pumped by diode lasers at 940 nm. The maximum incident pump intensity was 5.2 kW/cm², yielding an output intensity of 2.6 kW/cm² of multimode laser radiation. Rigrod analysis suggested that the laser operates with inhomogeneous gain saturation. Enhanced spatial hole burning in the active-mirror gain element is responsible for this effective inhomogeneous saturation. Full modulation of the intracavity intensity within the gain at the high reflector leads to poor gain extraction close to the intensity null regions and reduced effective gain length. The independence of the pump threshold and output intensities on the pump spot size indicates that the axial gain is not clamped by the transverse amplified spontaneous emission for up to a pump spot diameter of 18 mm. Observed thermal lensing contributions include thermal expansion–induced disk flexure, pump edge–induced temperature profile, and strong thermal imprint of the cooling nozzle due to the direct jet impingement on the high-reflection coated side. Weak absorption of the 1030-nm intracavity intensity in the undoped cap led to excess heating that limited the extracted intensity.

KEYWORDS: High power lasers, Yb:YAG, Thin disk laser

1. Background

Thin disk lasers are characterized by a gain media with a thickness that is significantly smaller than the pump beam diameter. The resulting one-dimensional thermal gradient across a 100- to 200-μm thick gain media leads to efficient axial heat extraction that minimizes thermally induced lensing and birefringence. In addition to paving the way

*Corresponding author; e-mail: william.latham@kirtland.af.mil.

[1]Dr. Lobad is currently a physics adjunct faculty member at Roger Williams University, Bristol, Rhode Island 02809.

for multikilowatt cw power scaling, thin disk lasers have allowed for the generation of subpicosecond pulse trains with record average powers exceeding 140 W[1] and energies per pulse of 26 μJ[2] directly out of an oscillator. The workhorse for much of thin-disk laser development has been Yb:YAG, which is a three-level laser system at room temperature with an Yb^{3+} lower-level split into four levels. The upper level is split into three levels, including a wide pumping band at 940 nm and a dominant lasing transition at 1.03 μm.[3–5] Single-crystal Yb:YAG thin-disk lasers (TDL) now operate at kilowatt powers with greater than 60% slope efficiencies and "wall-plug" efficiencies of more than 20%.[6–8] Further increase of the output power by scaling up the thin disk diameter from single-crystal boules beyond 2 cm is limited.[9] Recently, highly translucent and low scattering ceramic materials have been produced using purely chemical reactions and nanocrystalline powder sintering in vacuum ovens.[10,11] These advances promise several advantages over single-crystal laser materials, namely radially variable doping concentration profiles, composites, larger sizes, and potentially lower costs. Today, large-diameter polycrystalline Yb:YAG can be used for area scaling of single thin-disk lasers. Spectroscopic and laser characteristics of ceramic Yb:YAG are very similar to those of the single crystal but their superior mechanical strength makes them more favorable for high-power operation.[11] Low-power laser results with ceramics have been quite promising, with greater than 60% slope efficiency.[12] Taira et al. demonstrated output power intensity of 3.9 kW/cm^2 from a composite all-ceramic Yb:$Y_3Al_5O_{12}$ microchip laser with the maximum thermal stress exceeding twice the tensile strength of single-crystal YAG.[13] In this work, we demonstrate high-power scaling in ceramic Yb:YAG TDL, and investigate gain saturation, transverse amplified spontaneous emission (ASE), and thermal lensing contributions. Results illustrate that polycrystalline, Yb:YAG ceramic thin-disk geometry has strong potential for operation at the multikilowatt output level.

2. Thin Disks and Experimental Setup

Our capped Yb:YAG ceramic thin disks (TDs) consist of a 200-μm thick, 9.8%-doped, Yb:YAG layer diffusion bonded to a 1-mm undoped YAG ceramic. The top and bottom sides of the thin disk assembly are coated with a di-chroic antireflective (AR) and high-reflective (HR) coating, respectively, at both the 940-nm pump and the 1.03-μm laser wavelengths. The 37-mm disk is epoxied onto a 26-mm, clear-aperture Cu holder. The back of the disk is directly jet-impingement cooled (2.5 gal/min) at 20 °C. Fig. 1 shows IR and green upconverted fluorescence images of a pumped lasing and nonlasing (blocked cavity) TD. The cooling nozzle behind the disk is visible in the upconverted fluorescence images shown in Fig. 1(a) and (b), since the HR coating is not high reflecting for the green wavelength. TD scattering of the intracavity intensity is evident in the lasing TD IR fluorescence (Fig. 1(c)). Due to power extraction, the background fluorescence at both wavelengths is slightly dimmer in the lasing disk images of Fig. 1(a) and (c) than the corresponding blocked cavity images of Fig. 1(b) and (d).

The 940-nm laser diode pumping system, shown in Fig. 2(a), consisted of six Jenoptik 2.5-kW/25–bar-stack laser diodes with collimating spherical and cylindrical lenses combined using a thick polarizing plate and homogenized in a 20-cm InfraSil rod providing maximum pump power of 12.7 kW. The output of the homogenizing rod is relay-imaged to produce a fourth-order super-Gaussian pump profile. The pump beam is reimaged eight

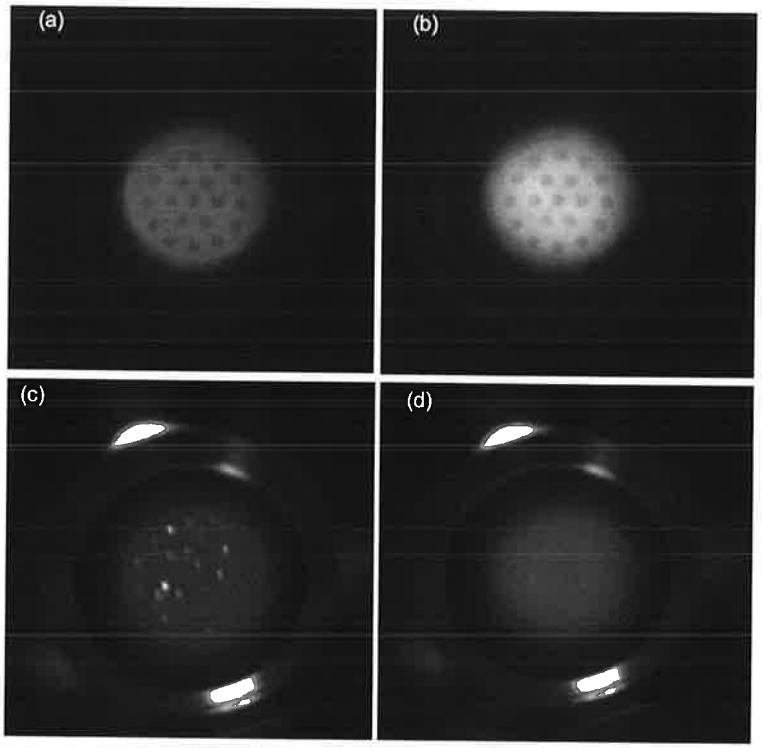

Fig. 1. Fluorescence images of TD under similar pump level. (a) Green upconverted fluorescence image under lasing condition. (b) Green fluorescence image with a blocked cavity. (c) IR fluorescence image under lasing condition. (d) IR fluorescence image with a blocked cavity. Image (c) shows scattering of the 1030-nm intracavity laser intensity at voids and/or inclusions in the thin disk. The intense spots are absent in the fluorescence mode in a blocked cavity (d) and the upconverted fluorescence images (a) and (b).

times on the thin disk using a parabolic mirror within the pump chamber, ensuring 90% absorption of the incident pump power (Fig. 2(b)). The absorbed pump power in the TD drops (saturates) to 80% in the fluorescence mode (blocked cavity). During multiple single-shot operations, the laser diode current was ramped over a 10-s period and held at the operating pump level for 5 s. This "ramping" was necessary to avoid overheating of the air-cooled, homogenizing InfraSil rod (>350 °C). The rod heating problem has been recently alleviated by using a Heraeus SupraSil rod with an order-of-magnitude lower absorption at 940 nm. The thermal diffusivity of YAG (4.5 mm^2/s) yields a thermal diffusion time constant of ~0.35 s in our 1.2-mm thick YAG composite structure. The actual time constant is much shorter considering that the heat generation occurs mostly in the 200-μm doped region. This ensures equilibrium lasing and thermal conditions during the ramp and hold operation. The ramp and hold time is shorter than the time constant of our large thermopile power meter (>40 s); therefore, a pickoff beam splitter and a large-area biased photodiode were used to measure the power. The photodiode was calibrated with the thermopile power meter at a cw output power of 500 W. A sudden drop in the slope efficiency during the ramp

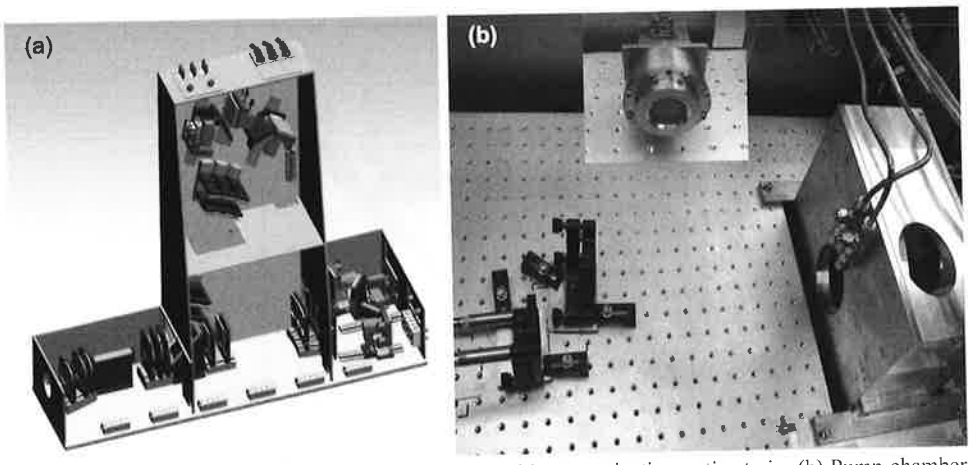

Fig. 2. (a) Diode pump conditioning, combination and homogenization optics train. (b) Pump chamber encloses the pump imaging parabolic and folding mirrors in a V-fold cavity. The disk cooling mount is shown in the insert.

stage or the output power during the hold was used to turn off the pump diodes in order to avert catastrophic damage to the thin disk or other optical elements.

3. Experimental Data and Analysis

To investigate and model the gain saturation in our thin disks, both a linear I-cavity (TD as an end cavity mirror) and folded V-cavity (TD as an internal-cavity folding mirror) were tested using 2-m radius of curvature (roc) output-coupling mirrors of 1 to 13% transmission. Measurements were performed for pump spot sizes of 11-mm and 18-mm diameter to quantify the role (if any) of transverse ASE in our capped thin disks. Thermal lensing of the thin disk was inferred using a probe laser beam; the deleterious effect of absorption on the intracavity laser intensity in the undoped cap is discussed at the end.

3.1. Output power and cavity stability

Figure 3 shows the output power and slope efficiency a as a function of pump power and intensity for both the V-fold cavity (at 4% output coupling) and the linear cavity (at 2% output coupling). The linear cavity achieved 6.5 kW output at ~60% slope efficiency while the V-fold cavity achieved a maximum of 5.5 kW, before a controlled shut down of the pump diodes was triggered by a sudden drop in the slope efficiency at a pump intensity of 4.5 kW/cm^2. This repeatable slope efficiency drop and shut-down was caused by cavity instability due to the thermal expansion–induced TD flexure. Stability analysis indicates that a disk radius of –3-m curvature makes the cavity unstable. This curvature estimate amounts to >20 waves of sag across the disk, which agrees with thermal lensing measurement of a 980-nm probe beam bouncing off the TD as will be shown below. As the size of the lowest cavity mode increases with TD flexure, the ratio of the pump spot size to that of the fundamental cavity mode decreases from ~10 at low pump power to ~7 before

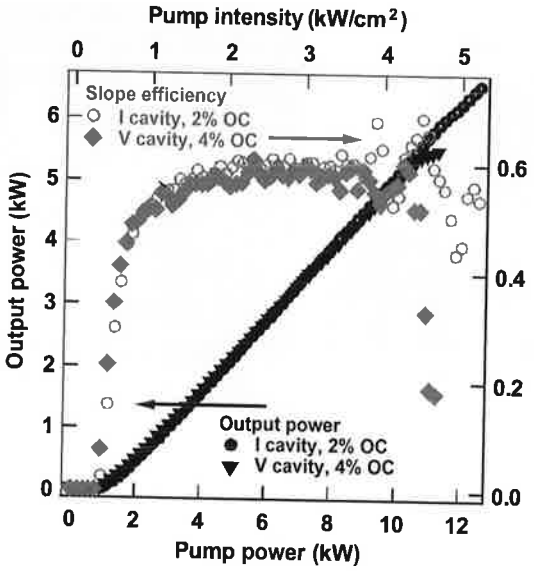

Fig. 3. Output power and slope efficiency measured during a 15-s ramp as a function of pump power and intensity for both V-fold (4% output coupling) and linear (2% output coupling) cavities.

the V-fold cavity became unstable. The linear cavity, on the other hand, should be stable up to a stronger disk curvature of –1.5 m due to the shorter cavity involving half the number of bounces off the thin disk per round trip compared to the V-fold cavity.

3.2. Rigrod, gain saturation, and cavity losses

The dependence of the output power intensity on the output-coupling fraction T_{oc} (Rigrod curve) and the pump parameter r (pump to threshold ratio) for the V and I cavities at a pump intensity of 2.72 kW/cm² are plotted in Fig. 4(a) and (b). The optimal transmission-output coupling (peak of the Rigrod curve) for the linear and V-fold cavities were 2% and 4%, respectively.

The four experimental curves of Fig. 4 were simultaneously fit using the following equations for the output intensity and pump parameter:

$$I_i(T_{OC}) = \frac{T_{OC}\, I_{sat}}{f_i}\left(r_i^n(T_{OC}) - 1\right) \tag{1}$$

$$r_i(T_{OC}) = \frac{Ln(G_i)}{Ln\left(\frac{1}{1-T_{OC}}\right) + Loss_i} \tag{2}$$

where $i = I$ or V representing both cavity types, $f_i = 3$ to account for the effect of a longitudinal spatial hole burning in standing-wave cavities, which Casperson has shown to reduce laser

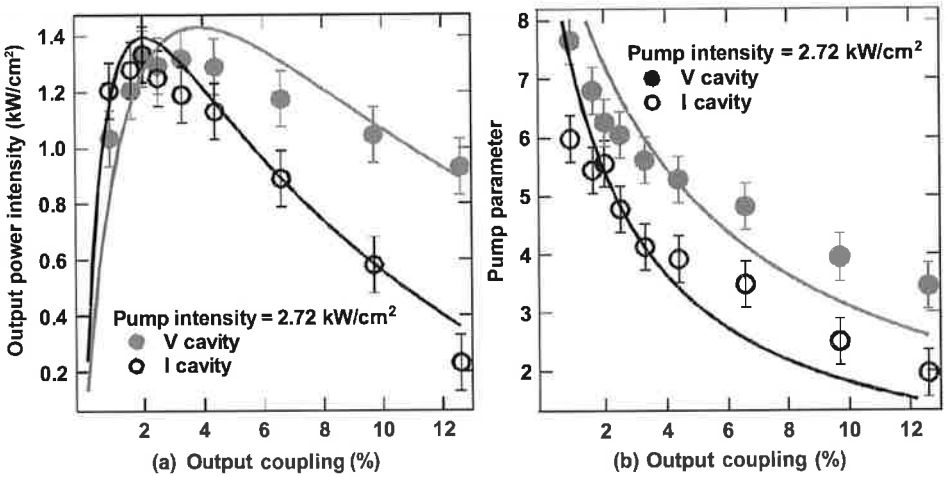

Fig. 4. (a) Rigrod and (b) pump parameter (pump to threshold ratio) curves for the V and I cavities at a pump intensity of 2.72 kW/cm², along with best-fit curves.

output power by ~30%[14] and $f_V = 2\,f_I$ since the intracavity intensity in a V-fold cavity saturates the gain twice in a single round trip. T_{OC} is the output coupling transmission, I_{sat} is the saturation intensity, and the exponent n represents effective saturation type, homogeneous ($n = 1$) versus inhomogeneous ($n = 2$).[14] The terms $Ln(G_i)$, $r_i(T_{OC})$, and $Loss_i$ represent the round-trip gain, pump parameter, and round-trip loss, respectively. The corresponding curve fits are imposed on the experimental data in Fig. 4 with fitting parameters $I_{sat} = 7.5$ kW/cm², $G_I = 1.26$, $G_V = 1.58$ (small signal gain $g_{ss} = 5.78$ cm^{-1}), $n = 1.99$, $Loss_I = 0.022$, and $Loss_V = 0.042$. The fit-extracted gain is consistent with small-signal gain measurement of a 1030-nm probe beam at low pump powers. The shift in the gain spectra to a higher wavelength prevented reliable gain measurement at higher pump powers. The V-fold cavity loss is roughly twice that of the linear cavity. This suggests that the majority of the loss being in the disk since the V-fold cavity has twice the number of passes through the disk per round trip.

Yb transition in YAG is known to be homogeneously broadened due to the strong coupling of the Yb ions through the YAG lattice phonons. This coupling leads to thermalization time scales on the order of picoseconds and the uniform saturation of the entire upper state energy manifold as a single line. Our results, on the other hand, suggest inhomogeneous gain saturation and indicate that a curve fit based on homogeneous saturation ($n = 1$) is not possible. Given the literature value of 9.7 kW/cm² for the saturation intensity and the measured pump parameter at the optimal output coupling of 2% for the I-cavity (Fig. 4(b)), the output intensity should be ~20% of what is measured in Fig. 4(a). Therefore, a curve fit based on homogeneous saturation can only be achieved by using an I_{sat} value in excess of 45 kW/cm² or using the square of the pump parameter ($n = 2$) suggesting much weaker saturation. The decreasing emission cross-section[15] at higher operating temperatures of up to 400 K would only increase the saturation intensity by up to 10%, which leaves standing the possibility of effective inhomogeneous saturation in our thin disk laser.

Inhomogeneous saturation in our thin disk laser is a consequence of the enhanced spatial hole burning (SHB) within the active mirror configuration. This effect was observed

by Braun et al.[16] and modeled by Kartner et al.,[17] where they have shown that under CW operation a Nd:YLF gain crystal saturates homogeneously in a single longitudinal line when placed in the middle of the cavity, and saturates inhomogeneously, with multiple longitudinal modes, when in an active mirror configuration at the end of the cavity. As evidence for effective inhomogeneous saturation, the number of longitudinal lasing modes was observed to increase with the pump parameter. The global null condition at the HR coating for all lasing modes leads to full modulation of the intracavity intensity (separated by $\lambda/2n \sim 0.3$ μm) that decays axially toward the AR side. The unextracted gain at those intracavity intensity nulls allows more longitudinal modes to lase. Braun et al. also showed that in mode-locked operation, this effective inhomogeneous broadening leads to significant broadening of the pulse bandwidth resulting in shorter pulse widths for active gain mirror configuration.[16]

The seemingly high loss in our disks is consistent with the optimal output coupling inferred from Fig. 4(a) for an inhomogeneously broadened laser. By equating the derivative of Eq. (1) (for $n = 2$) to zero and solving for optimum T_{OC}, one can show that the cavity loss is always larger than the optimum output coupling. In our case, the difference between cavity losses and the optimum coupling is given by $(Loss - T_{OC\text{-}Opt}) = (Loss + T_{OC\text{-}Opt})^3/Ln(G) \sim 0.03\%$. This is in contrast to the homogeneous saturation case where $T_{OC\text{-}Opt} > Loss$. This loss is attributed to absorption in the undoped cap and AR coating (Fig. 7 below), and to scattering off of inclusions and voids in the diffusion layer as evident in Fig. 1(c).

In deriving the effect of longitudinal SHB ($f_l = 3$) only the conventional SHB was considered.[14] In the case of enhanced SHB, the global null condition imposed at the HR coating on all lasing modes leads to stronger intracavity intensity modulation within the thin gain element, and a stronger reduction in the output power than that produced by the conventional SHB effect in a gain element in the middle of the cavity with weaker intensity modulation. We expect that taking into account this stronger reduction in output power results in a larger saturation intensity fit parameter and a better agreement with the literature value of 9.7 kW/cm^2. It is worth noting that fitting our data using the literature value for the saturation intensity is possible only with a 7% increase in the chi-square fit error. On the other hand, forcing a homogeneous saturation fit ($n = 1$) leads to an excessively high $I_{sat} \sim 50$ kW/cm^2 and much worse fit with a ~150% increase in the chi-square fit error. We attribute the poor fit of Fig. 4 to the overly simplistic model used, which is accurate at low output couplings and becomes inadequate at the higher output couplings used.

In support of effective inhomogeneous saturation, we observed simultaneous multiwavelength lasing at 1030 nm and 1049 nm. This was observed only with the lowest output-coupling transmission "loss" (1%) and the higher-gain V-fold cavity. Heating-induced reabsorption suppresses the gain at 1030 nm more strongly than at 1049 nm, which has a scarcely populated ground state in comparison to the lower energy ground state of the 1030-nm transition. Similar observations were reported by Dong et al. in the Yb:YAG 1-mm microchip laser.[18] Dong et al. resolved multiple (up to seven) longitudinal modes lasing in both the 1030-nm and 1049-nm bands. The 1049-nm operation in their multiwatt-level, 1-mm thick microchip laser occurs over a wider range of pumping and output coupling conditions.[18] This is due to the lack of active cooling, which results in significant gain reduction at 1030 nm due to the increase in the lower lasing level population.

Axial modulation leads to a longitudinal mode separation that is determined by the gain thickness rather than the cavity length.[16,17] In a 200-μm thick gain, the lasing longitudinal

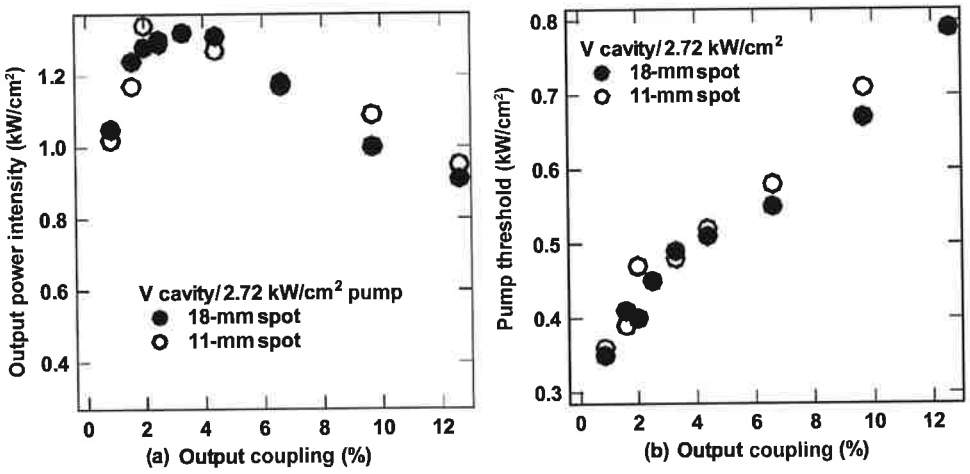

Fig. 5. (a) Rigrod curves and (b) threshold pump intensities for 11-mm and 18-mm pump spot sizes in the V-fold cavity configuration as a function of output coupling fraction for an equivalent pump intensity of 2.72 kW/cm^2.

mode separation is ~415 GHz, instead of ~150 MHz for a 1-m cavity, which means there are only about five longitudinal modes within the gain bandwidth. This limited number of modes reflects quasi-inhomogeneous saturation in the homogenously broadened Yb:YAG, and ensures that intracavity intensity modulation persists for most of the short gain length. Along the axial intensity null positions, there is no gain extraction and the pump energy is lost to fluorescence leading to poor gain extraction and an effectively shorter gain thickness. The maximum possible gain for full inversion of the Yb dopants is ~29.12 cm^{-1}, given by the product of the stimulated emission cross-section and the doping concentration. At a pump level of 2.72 kW/cm^2, and assuming 90% of the incident photons are absorbed, we expect 42% of the dopant atoms to be inverted resulting in a gain of ~12.5 cm^{-1}. This estimate is twice the fit-extracted gain of 5.78 cm^{-1}, which is evidence of a shorter effective gain length.

3.3. Transverse ASE and the undoped cap

The observed gain reduction can also be attributed to concentration quenching or transverse amplified spontaneous emission (ASE). Concentration quenching is known to be of concern at higher (>15%) doping concentrations.[19,20] The thin disks used in this work are doped at 9.8%; therefore, concentration quenching is not expected to play a role. Transverse amplified spontaneous emission in our TD is mitigated by the undoped cap layer. By providing refractive index matching, the undoped cap serves to prevent the trapping and amplification of spontaneous emission that may otherwise occur through total internal reflection within the 200-μm gain region. To quantify the role of transverse ASE in our disk, we measured the Rigrod curves for two pump spot sizes. The V-fold cavity output power intensity, for 11-mm and 18-mm pump spot sizes, is plotted in Fig. 5(a) as a function of output coupling under an equivalent pump intensity of 2.72 kW/cm^2.

The dependence of the threshold pump intensity for both pump spot sizes on the output coupling is shown in Fig. 5(b). No discernible difference between the two pump spot sizes is observed, especially up to the high output coupling, which suggests that transverse ASE is not competing with axial cavity gain despite more than an order of magnitude ratio of the transverse to axial dimensions of the pumped gain region. The role of the undoped cap in the scaling of thin disk lasers was modeled by Kouznetsov et al.[21] for a disk of thickness h and transverse dimension L. In this case, only a small fraction of the ASE directed into an angle of order h/L propagates in the plane of the disk and is amplified. This amplified ASE should reduce lifetime by an upper limit factor of $(h/L)*exp(GL)$, which amounts to 10% and 7% for the 18-mm and 11-mm pump spot diameters, respectively. This lifetime reduction is not evident in Fig. 5, and does not explain the factor-of-2 reduction between the estimated and the fit-extracted gain value.

3.4. Thermal lensing

Thermal lensing of the lasing disk was measured using an expanded and collimated 980-nm, fiber-coupled, semiconductor laser probe beam. The far-field beam profile was imaged on a camera 2.2 m away from the thin disk. Three thermal lensing contributions were identified: (1) thermal expansion–induced negative lensing (disk acquires a convex roc), (2) positive lensing due to the radial temperature profile toward the pump-spot edge, and (3) thermal imprint of the cooling nozzle. The far-field profile of the 7-mm diameter probe beam reflecting off the unpumped disk is shown in Fig. 6(a) together with the outline of the 11-mm and 18-mm pump spots. Figs. 6(b) and (c) show the probe profile off of the pumped disk for the small and large pump spots of equal pump intensity, respectively. Positive lensing due to the radial pump-edge temperature profile is evident in the intense ring and the smaller focused probe beam in Fig. 6(b). Thermal expansion–induced negative lensing and the nozzle imprint are clearly displayed for the large pump spot in Fig. 6(c). For the 18-mm pump beam, the probe beam is too small to sample radial temperature gradients at the edge of the pump spot. It is worth pointing out that thermal expansion–induced disk flexure scales with the total pump power and not with pump intensity. For that reason, the V-fold cavity becomes unstable at a pump intensity of 4.5 kW/cm^2 for the 18-mm pump spot, while for the smaller 11-mm pump spot the cavity is stable for pump intensities exceeding 6 kW/cm^2.

A fluid-flow and thermal-conduction simulation (using CFdesign software) of our jet impingement cooling nozzle showed strong transverse variation of the water velocity and film coefficient. Under a heat load of 0.8 kW/cm^2, this transverse variation translates to temperature variations of up to 40 °C between directly jet-cooled locations and locations between jets. The simulation points to complete washout of this transverse temperature variation on the interior of the undoped cap due to radial heat conduction. This is in agreement with the absence of transverse temperature variation in thermal camera images of the undoped cap (not shown). The pump-induced nozzle thermal imprint is fully developed at a distance of ~30 cm from the disk. This pattern has complicated proper wavefront characterization. It has been reported that the nozzle thermal imprint is invisible using a 1064-nm probe on similar disks cooled with direct jet impingement. Such results suggest that this effect can be eliminated by optimizing the jet parameters.[22] Our jet holes were h ~ 0.9 mm in diameter drilled in a cone-shaped plate with a full cone angle of 160 degrees

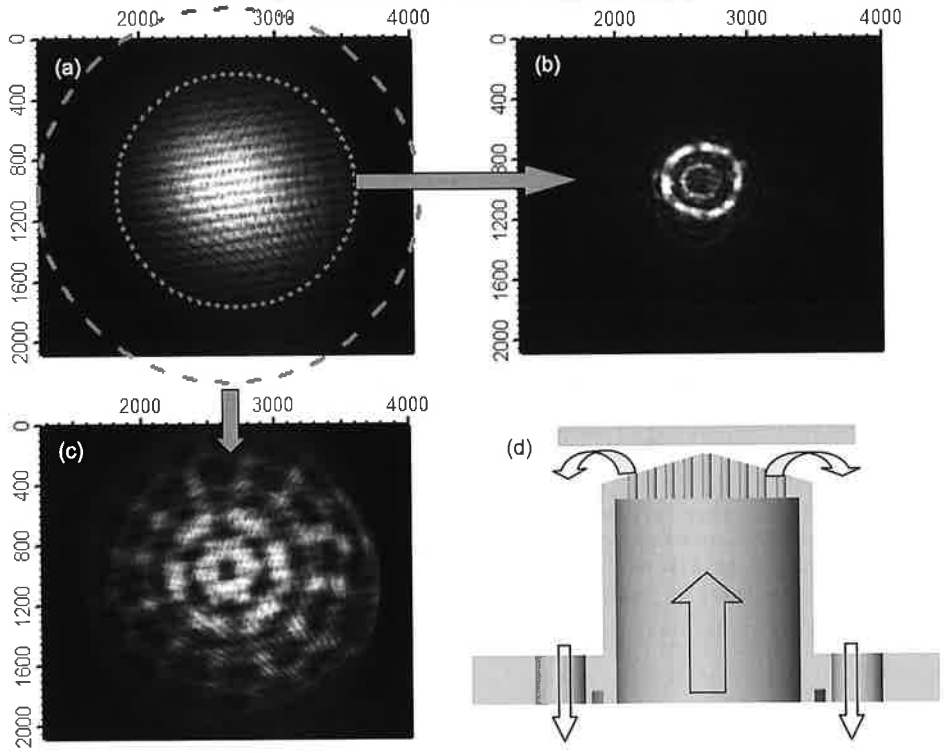

Fig. 6. (a) Far-field profile of a 7-mm diameter, 980-nm probe beam reflecting off the unpumped disk together with the outline of the 11-mm (dotted circle) and 18-mm (dashed circle) pump spots. Figures (b) and (c) show the probe profile off the pumped disk for small and large pump spots, respectively, for equal pump intensity. (d) Jet impingement nozzle design and its position in relation to thin disk.

as shown in Fig. 6(d). The exit point for the center hole was $d \sim 0.7$ mm distance from the HR coating, and the thickness of the plate for that hole was $p \sim 3.25$ mm. The combination of $h \sim d$ and $p > d$ probably resulted in collimated jets hitting the disk with a small cone angle and generating a thermal imprint due to inadequate flow overlap for neighboring jets at the disk.

3.5. Intracavity absorption and TD heating

The temperature of the undoped cap, measured by a thermal camera operating in the 10-μm band, was systematically higher in the lasing mode than in the nonlasing/fluorescence mode (blocked cavity). The rate of temperature increase (heating slope) in degrees Centigrade per kilowatt per square centimeter of absorbed pump intensity at the AR-coated side of the 1-mm, undoped bonded cap is plotted for both I and V cavities in Fig. 7 as a function of the output coupling fraction. The fluorescence-mode heating slope of 23.8 °C/(kW/cm^2)